3D differential phase-contrast microscopy with computational illumination using an LED array

Lei Tian,* Jingyan Wang, and Laura Waller

Department of Electrical Engineering and Computer Sciences, University of California, Berkeley, California, USA
*Corresponding author: lei_tian@alum.mit.edu

We demonstrate 3D differential phase-contrast (DPC) microscopy, based on computational illumination with a programmable LED array. By capturing intensity images with various illumination angles generated by sequentially patterning an LED array source, we digitally refocus images through various depths via light field processing. The intensity differences from images taken at complementary illumination angles are then used to generate DPC images, which are related to the gradient of phase. The proposed method achieves 3D DPC with simple, inexpensive optics and no moving parts. We experimentally demonstrate our method by imaging a camel hair sample in 3D.   © 2014 Optical Society of America

OCIS codes: (170.6900) Three-dimensional microscopy; (110.1758) Computational imaging; (100.5070) Phase retrieval.
http://dx.doi.org/10.1364/OL.39.001326

Computational imaging involves the joint design of optical systems and post-processing algorithms for new imaging capabilities (e.g., phase, 3D, super-resolution). Most previous work involves detection side coding, in which an optical element is placed between the sample and the camera. Here we employ computational illumination, where the coding is instead done on the illumination side. Distinct from structured illumination, which patterns object space, we work with a coded source plane in Köhler configuration (Fourier space). Such a system generates homogenous intensity across the sample, but with coded angles. Our experimental setup is inspired by recent work in which a microscope lamp is replaced by a programmable LED array [1,2]. This single hardware platform enables any of the bright field, dark field, digital refocused, or super-resolution modalities, simply by choosing the LED pattern at the source. Here we describe how this system can also incorporate phase contrast capabilities in 3D without any hardware changes.

Phase imaging is an important tool for biological research, as it provides label-free contrast for transparent samples. Commercial microscopes generally employ either phase contrast (PhC) or differential interference contrast (DIC), both of which require expensive hardware inserts. Here we make use of a phase-imaging method that requires only two images illuminated by complementary angles, known as differential phase contrast (DPC) [3–5]. It does not rely on specialized objectives (like PhC) or polarization optics (like DIC), so it is more suitable for imaging birefringent specimens [5]. The same technique has been recently adapted to reflection geometry for imaging thick tissue [6]. We show here an adaptation on DPC that extends its capabilities to computational refocusing for 3D phase contrast.

DPC works under the principle that the gradient of phase can be extracted from a pair of intensity images taken with opposite illumination angles (e.g., one with the left side of the source on, I_L, and one with the right side of the source on, I_R). The DPC image is then computed as the normalized difference between the images:

$$I_{DPC} = (I_L - I_R)/I_{tot}, \tag{1}$$

where $I_{tot} = I_L + I_R$ is the sum of the images (a brightfield image). Consider a thin amplitude object in focus. Illuminating from either side does not change the intensity ($I_L = I_R$), since a purely real object has a symmetric Fourier transform. Thus the image computed by Eq. (1) will contain no amplitude information from the focal plane. Phase variations, however, cause local changes in propagation direction [7], and the difference between the images I_L and I_R is related to the object's phase gradient along the axis of asymmetry [3]. In principle, these images could be inverted to recover quantitative phase (unlike standard DIC or PhC).

The experimental setup is illustrated in Fig. 1. The microscope consists of a 10× (0.25 NA) objective, a 100 mm focal length tube lens, and a CMOS camera (Thorlabs DCC1240C). An LED array (Adafruit 607) is placed at the back focal plane of the condenser lens (⌀75 mm, focal length $f = 60$ mm) and controlled by an Arduino. Each LED illuminates the sample from a unique angle set by its spatial location. In this geometry, only the central 45 LEDs generate illumination angles within the NA of the objective (termed "brightfield LEDs"), while those outside this circle correspond to dark field illumination. We consider only the brightfield LEDs here.
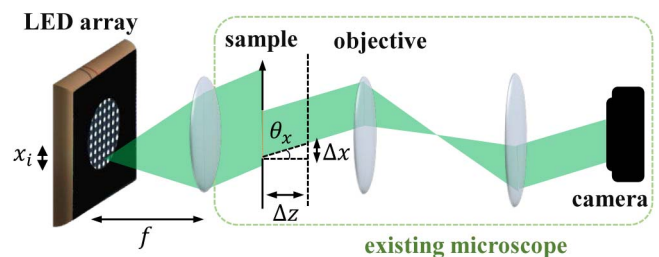

Fig. 1. Experimental setup. A programmable LED array is placed at the back focal plane of the condenser. Each LED generates illumination at a different oblique angle, corresponding to its spatial location in the array.
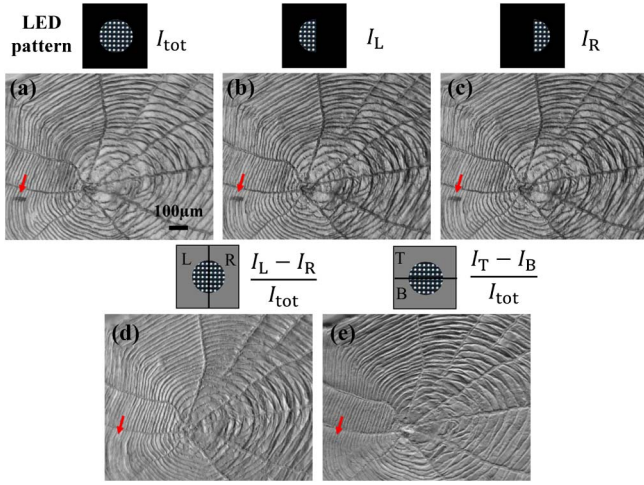
© 2014 Optical Society of America

Fig. 2.   (a) A fishscale sample is imaged with all the brightfield LEDs on and then with only (b) the left-half LEDs and (c) the right-half LEDs on. (d) The left–right DPC image is computed from (a) and (b). (e) The top–bottom DPC image is obtained by repeating the same process on images taken with top and bottom halves on.

To test DPC in our system, we first image a thin fish-scale sample. As shown in the brightfield image (all brightfield LEDs on) in Fig. 2(a), the sample contains grid-like structures at different orientations, which is convenient for demonstrating the directional information contained in DPC. We obtain DPC images by capturing two images sequentially, each with opposite halves of the brightfield LEDs on [Figs. 2(b) and 2(c)] and then computing the DPC image using Eq. (1). The same process may be repeated for arbitrary orientation of the axis of asymmetry, without mechanical rotation; we show here only left-right and top–bottom DPC images in Figs. 2(d) and 2(e), respectively. The DPC images correspond to the phase gradient along the direction of asymmetry and therefore display a shadowing effect along that direction, similar to DIC. In contrast to DIC (and PhC), DPC images do not contain mixed phase and amplitude information from the focal plane. For example, the dust particle (indicated by a red arrow in the bottom-left corner of the brightfield image), which is a pure amplitude object, does not show up in the DPC image.

In order to recover 3D phase information, one can physically scan axial distances [4–8] or illumination angles [9]. In our setup, we sequentially scan through the 2D array of LEDs, corresponding to scanning of the illumination angle in both lateral directions and limited only by the NA of the objective. The angle of illumination (θ_x, θ_y) is related to the coordinates of the LED, (x_i, y_i) by $\tan\theta_x = x_i/f$ and $\tan\theta_y = y_i/f$. This collected data can then be processed with light field methods that digitally refocus the images to various depths [1]. The images correspond to a 4D data matrix of two spatial and two angular variables, similar to that of a light field camera. With this dataset, we use a simple shift-and-add process [10], which removes geometric defocus effects corresponding to a spherical spread of intensity. For a reconstructed depth at a distance Δz from the actual focal plane, each image (corresponding to each LED) is shifted by $\Delta x = \Delta z \tan\theta_x$, $\Delta y = \Delta z \tan\theta_y$ (Fig. 1),
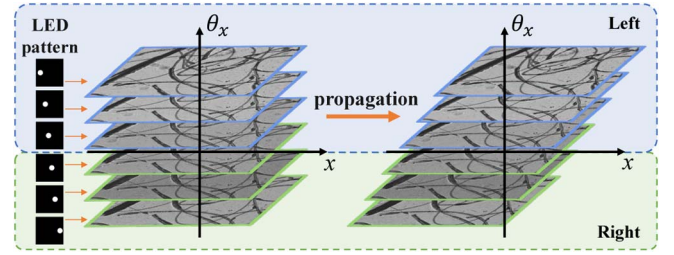

Fig. 3.   3D camel hair sample is illuminated by different LEDs corresponding to different illumination angles. To synthesize intensity at a different focus plane, each image is shifted by an amount proportional to the illumination angle. The shift-and-add process shears the 4D matrix, then integrates across all angles. In order to get DPC images for each synthesized focal plane, we separately add the images corresponding to left and right sides of the source plane. [Online: movie shows images for each brightfield LED (Media 1)]

and then all the shifted images are added together. This is akin to the 4D shearing process of light field digital re-focusing; larger angles and/or depths result in larger shifts (see Fig. 3).

Our algorithm for extending the light field refocusing methods to 3D DPC involves four steps. First, we collect intensity images by sequentially scanning through the brightfield LEDs. Second, all images are shifted according to the desired refocusing distance. Third, we need to add the shifted images to obtain the refocused image. In light field processing, all shifted images are summed, akin to a projection across angles. Here, we instead synthesize the defocused intensity image with only one half of the bright field LEDs on by simply adding the corresponding shifted images (only those corresponding to the LEDs in one half of the source plane). As illustrated in Fig. 3, defocus introduces a shift only in the spatial dimension x, not in the angle θ_x, making this possible. For example, the intensity image $I_L^{\Delta z}$ at the focal plane Δz with the left half of the brightfield LEDs on as the synthesized illumination pattern can be calculated as

$$I_L^{\Delta z} = \sum_{\text{left half of bright field LEDs}} I_i^{\Delta z}, \qquad (2)$$

where $I_i^{\Delta z}$ denotes the shifted intensity image at Δz from the ith LED. The same process is repeated for the right half of the brightfield LEDs, $I_R^{\Delta z}$. Finally the DPC equation [Eq. (1)] is applied to the synthesized complementary images to compute the defocused DPC image. The DPC image at the focal plane Δz is

$$I_{DPC}^{\Delta z} = (I_L^{\Delta z} - I_R^{\Delta z})/I_{tot}^{\Delta z}, \qquad (3)$$

where $I_{tot}^{\Delta z} = \sum_{\text{all bright field LEDs}} I_i^{\Delta z}$ is the refocused bright field image.

We verify our 3D DPC method by imaging a thick sample consisting of camel hairs. Some raw images are shown in Fig. 3 for LEDs illuminating with varying θ_x. The entire dataset is taken with 4.5 s exposure time (100 ms for each LED). The perspective of the sample changes with illumination angle, clearly seen in Media 1. Three-dimensional DPC results are computed from the experimental data, and the results are shown in Fig. 4 and
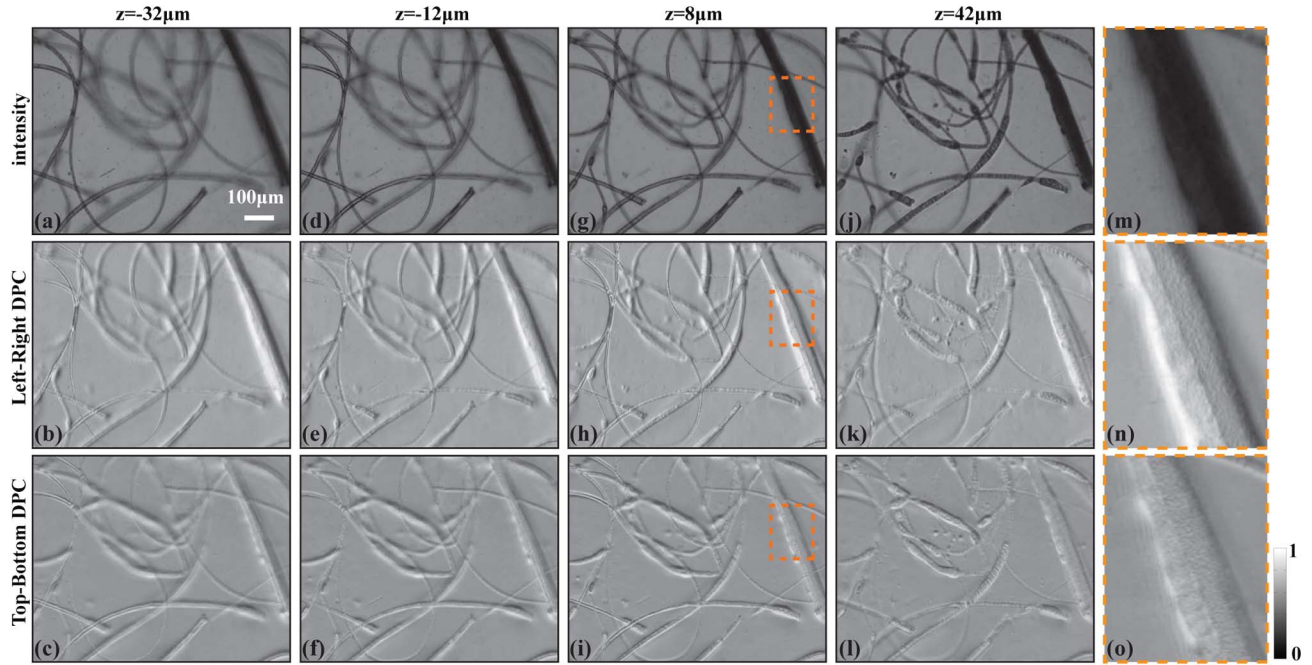
Fig. 4.   Experimental results for 3D DPC. (a), (d), (g), (j), (m) Digitally refocused intensities. (b), (e), (h), (k), (n) Left–right DPC images. (c), (f), (i), (l), (o) Top–bottom DPC images at (a)–(c) $z = -32$ μm, (d)–(f) $z = -12$ μm, (g)–(i) $z = 8$ μm, and (j)–(l) $z = 42$ μm. (m)–(o) Magnified images from regions within the dotted orange rectangles. [Online: movies of 3D slices of intensity and DPC images from −100 μm to 100 μm with 3 μm increment (Media 2).]

Media 2. The digitally refocused DPC images corresponding to phase gradients along the horizontal and vertical directions are shown, with comparison to the digitally refocused brightfield intensity images at the same synthesized focal planes. As highlighted in the zoom-in of Fig. 4(m)–4(o), features that do not have good contrast in the intensity images often show up nicely in the DPC images. In similarity to PhC and DIC, our DPC images also have a somewhat high-pass filtered appearance, which results from the gradient effect (a ramp in Fourier space); low frequencies are attenuated, while high frequencies are accentuated.

Our depth resolution will be limited by the depth-sectioning capabilities of the microscope (set by the NA of the objective). Because of imperfect depth sectioning, both in-focus and out-of-focus features of the 3D object contribute to the brightfield intensity and also to the DPC image. This effect can be described by a convolution of the 3D object with the 3D point spread function (PSF) [11]. Thus, slightly out-of-focus amplitude objects may have a defocus-induced phase component, which shows up in the DPC image. This is a real effect and also appears in physically refocused DPC images [4]. It is thus not accounted for in our algorithm, but could be mitigated by 3D deconvolution in post-processing. Our brightfield images follow the general rule of thumb, having depth sectioning λ/NA^2. However, when the illumination NA is smaller than the imaging NA (not all LEDs inside brightfield region used), there will be less depth sectioning. In Fig. 5, we demonstrate this controllable depth-sectioning capability by illuminating with circles of varying radii. This is equivalent to varying the condenser aperture size in a traditional microscope in order to control the (in)coherence parameter $\sigma = \mathrm{NA}_{\mathrm{illumination}}/\mathrm{NA}_{\mathrm{objective}}$.

As expected, increasing σ increases depth sectioning, up to the limit of the imaging system NA. When the sample is illuminated by a single LED, objects from all depths appear in focus and diffraction ringing is visible, due to the relatively high spatial coherence. As σ increases (more LEDs are turned on), depth sectioning improves and interference effects are washed out. The same trends follow in our DPC images. Since many single-LED images are added in order to compute each DPC image, the final result effectively has reduced coherence. Thus our algorithm is tolerant to diffraction, even though we do not explicitly consider coherence in the reconstruction. Interestingly, the DPC images appear to have better depth sectioning than bright field images. This is due to the attenuation of low spatial frequencies [8], which change less through focus because of their associated small angles.
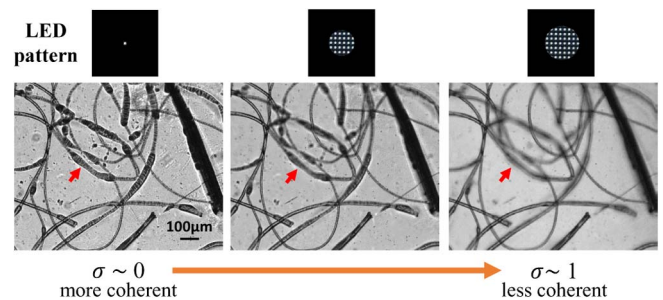

Fig. 5.   Images taken with increasing radii of LED illumination corresponding to increased σ from almost zero to one. The features indicated by the red arrows appear in focus with large coherence, but blur out as more LEDs are turned on, indicating better optical sectioning.
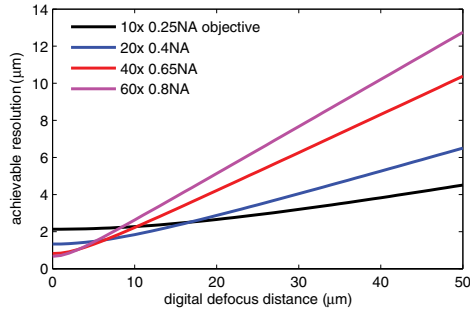
Fig. 6.   Lateral resolution degrades with increased digital defocus distance, due to unaccounted for broadening of the PSF in our algorithm. We plot here the theoretically achievable lateral resolution as a function of the distance between the synthetic focus plane and the actual focus plane for typical microscope objective properties.

One unwanted effect introduced by digital refocusing is a slight loss of resolution at synthesized focal planes, due to broadening of the PSF away from the actual focal plane. Based on the assumption that the broadening can be approximated by Gaussian spreading, we calculate the theoretically achievable lateral resolution as a function of defocus distance, shown in Fig. 6 for typical microscope objectives. It is seen that with the 0.25 NA objective used in our system, the resolution remains better than 5 μm within a ±50 μm refocus range. The achievable refocusing range will be determined by the desired resolution within the volume of interest. This loss of resolution could also be alleviated by 3D deconvolution [10,12] and will be considered in future work.

Our method is related to previous work in light field microscopy [10] in that it also captures 4D data with two spatial and two angular dimensions. The light field microscope offers single-shot capture, at the cost of trading spatial resolution for angular information [12]. Spatial resolution is critically important in microscopy, and our system has the advantage of always providing full spatial sampling, with the angular sampling being determined by the LED scanning. Conveniently, our LED array setup implements this scanning in near real-time and with no moving parts. Depth resolution and refocusing range are

set by the choice of angles (LEDs) and can be optimized for any given experiment. This offers a flexible trade-off between speed of capture and depth capability, while maintaining good spatial resolution.

To conclude, we have introduced 3D phase-contrast capabilities for an LED array microscope, which offers a flexible platform for various imaging modalities. Our system fits within a larger class of computational illumination schemes that pattern subsets of the 4D light field [13] or spatial coherence function [14]. Here we pattern only the 2D angle dimension of the 4D space-angle function and show how angular information can be used for computing DPC images at varying focal planes. Our system is simple, inexpensive, and achieves large illumination angles, without mechanical scanning.

References

1. G. Zheng, C. Kolner, and C. Yang, Opt. Lett. **36**, 3987 (2011).
2. G. Zheng, R. Horstmeyer, and C. Yang, Nat. Photonics **7**, 739 (2013).
3. D. Hamilton and C. Sheppard, J. Microsc. **133**, 27 (1984).
4. W. Amos, S. Reichelt, D. Cattermole, and J. Laufer, J. Microsc. **210**, 166 (2003).
5. S. B. Mehta and C. J. Sheppard, Opt. Lett. **34**, 1924 (2009).
6. T. N. Ford, K. K. Chu, and J. Mertz, Nat. Methods **9**, 1195 (2012).
7. B. C. Platt and R. Shack, J. Refrac. Surg. **17**, S573 (2001).
8. J. D. Giese, T. N. Ford, and J. Mertz, Opt. Express **22**, 1152 (2014).
9. W. Choi, C. Fang-Yen, K. Badizadegan, S. Oh, N. Lue, R. Dasari, and M. Feld, Nat. Methods **4**, 717 (2007).
10. M. Levoy, R. Ng, A. Adams, M. Footer, and M. Horowitz, ACM Trans. Graph. **25**, 924 (2006).
11. B. R. Frieden, J. Opt. Soc. Am. **57**, 56 (1967).
12. M. Broxton, L. Grosenick, S. Yang, N. Cohen, A. Andalman, K. Deisseroth, and M. Levoy, Opt. Express **21**, 25418 (2013).
13. M. Levoy, Z. Zhang, and I. McDowall, J. Microsc. **235**, 144 (2009).
14. L. Waller, G. Situ, and J. Fleischer, Nat. Photonics **6**, 474 (2012).